ARTICLE

Transparent Conductive Single-Walled Carbon Nanotube Networks with Precisely Tunable Ratios of Semiconducting and Metallic Nanotubes

Jeffrey L. Blackburn,* Teresa M. Barnes, Matthew C. Beard, Yong-Hyun Kim, Robert C. Tenent, Timothy J. McDonald, Bobby To, Timothy J. Coutts, and Michael J. Heben

National Renewable Energy Laboratory, Golden, Colorado 80401

ABSTRACT We present a comprehensive study of the optical and electrical properties of transparent conductive films made from precisely tuned ratios of metallic and semiconducting single-wall carbon nanotubes. The conductivity and transparency of the SWNT films are controlled by an interplay between localized and delocalized carriers, as determined by the SWNT electronic structure, tube−tube junctions, and intentional and unintentional redox dopants. The results suggest that the main resistance in the SWNT thin films is the resistance associated with tube−tube junctions. Redox dopants are found to increase the delocalized carrier density and transmission probability through intertube junctions more effectively for semiconductor-enriched films than for metal-enriched films. As a result, redox-doped semiconductor-enriched films are more conductive than either intrinsic or redox-doped metal-enriched films.

KEYWORDS: carbon nanotubes · conductivity · photovoltaic · doping · separation · thin films · optical properties · electrical properties

Transparent, conductive thin films of single-walled carbon nanotubes (SWNTs) are being studied extensively for possible application in solution-processed solar cells,[1−3] field-effect transistors,[4−6] touch-screens, and EMI shielding.[7] SWNT films are particularly attractive replacements for traditional transparent conductors such as indium tin oxide (ITO) in low-cost, flexible, or solution-processed applications due to the natural abundance of carbon, amenability to spraying and printing, and good wetting properties. However, despite several recent reports of organic and inorganic solar cells deposited on conductive SWNT films,[2,3] the efficiencies of similar ITO- or ZnO-based cells are not easily surpassed. For comparable or improved solar cell performance, SWNT thin films must meet or exceed the low sheet resistance values of high quality ITO, ∼5−10 Ω/sq, at comparable transparencies, ∼85%, across the visible electromagnetic spectrum.

SWNT thin films are three-dimensional interconnected networks of quantum wires, and a large number of factors can affect their optical and electrical properties. These factors include the intrinsic electrical resistance of the individual SWNTs within the network, the resistance associated with junctions between SWNTs,[8,9] and the tube-specific optical properties. One must also consider the degree to which intentional[10] and unintentional[11] redox doping modifies the optical and transport properties. Underlying all of these issues is the fact that as-produced SWNTs are polydisperse in their electronic structure, naturally consisting of ∼2/3 semiconducting (s-SWNTs) and 1/3 metallic (m-SWNTs) nanotubes. Due to this complexity, a detailed understanding of the phenomena that control the overall optical and transport properties of thin, transparent SWNT films has not yet emerged. In fact, it is not clear whether a film formed solely with m-SWNTs would be a better transparent conductor than a film formed solely with s-SWNTs. Naively, one might expect that metals would be better for optimizing conductivity in the films, while semiconductors might be better for transparency. However, what composition should one use to simultaneously optimize both characteristics?

While reports exist on the conductivity of single s- or m-SWNTs,[4,5] single-tube transport studies yield idealized transport parameters that may not be applicable to thin film geometries where the tube−tube interfaces may be quite important. Also, it is difficult to integrate optical measurement techniques with these studies. Transparent films and opaque mats (*i.e.*, "bucky papers")

*Address correspondence to jeffrey_blackburn@nrel.gov.

Received for review March 27, 2008 and accepted May 05, 2008.

Published online May 29, 2008.
10.1021/nn800200d CCC: $40.75

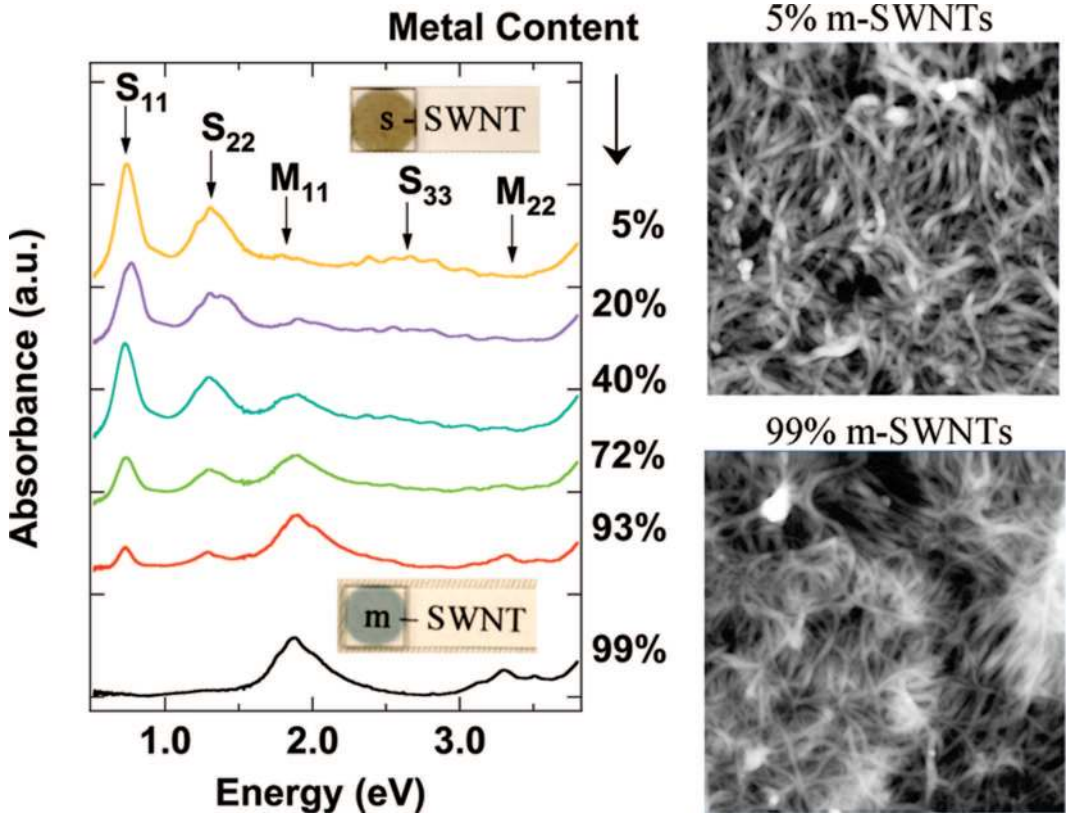

Figure 1. (Left panel) Corrected absorbance spectra of a range of films with varying m- and s-SWNT contents. For clarity, the spectra have had the rising ultraviolet background subtracted to produce a relatively flat background in the range of 0.5 to 4 eV, based upon the procedure of Nair *et al.*[19] Insets show pictures of semiconductor-enriched and metal-enriched SWNT transparent films. (Right panels) 2 × 2 μm AFM images of semiconductor-enriched (top right) and metal-enriched (bottom right) transparent SWNT films.

of bulk, as-produced SWNTs have been studied,[12–14] but these investigations were performed with mixtures of m- and s-SWNTs. Also, opaque mats have nanotube densities far exceeding the percolation threshold and are poorly suited to solar applications where transparency is critical. Only one recent report has studied a metal-enriched transparent SWNT film.[15] A comparison was made to a film prepared from as-produced SWNTs, and the study focused on the stability of the film's optical properties rather than on mechanistic issues.

Here we examine the optical and electrical properties of transparent, conductive SWNT films that were purposefully produced with precisely tuned ratios of s- and m-SWNTs. A combination of optical spectroscopy and conductivity measurements allows us to carefully evaluate the impacts of SWNT electronic structure and redox doping on the intrinsic SWNT resistance, junction resistance, and ultimate performance of these thin film electrodes. A wide range of film compositions were studied, from 99% m-SWNT to 95% s-SWNT. Ultimately, we find superior performance in redox-doped semiconductor-enriched films due to dramatic redox-induced changes in the carrier density barrier properties, and the delocalization of carrier density.

SWNT solutions enriched in m- or s-SWNTs were prepared by density gradient centrifugation, as described by Arnold *et al.*[16] Following density gradient ultracentrifugation, successive aliquots were removed from the density gradient. These aliquots contain a variable proportion of m- and s-SWNTs, according to their position in the density gradient and the amount of unintentional mixing. We estimate the relative proportions of m- and s-SWNTs in solution by comparing the integrated areas of the first metallic (M_{11}) and second semiconducting (S_{22}) transitions in the visible absorbance spectrum (Supporting Information).[17] We then combined the appropriate volumes of specifically chosen fractions to prepare films, *via* vacuum filtration,[18] having a wide range of precisely controllable metal/semiconductor ratios.

Figure 1 shows background-subtracted[19] UV−vis−IR spectra for a series of transparent SWNT films with varying m- and s-SWNT contents. The peak envelopes corresponding to intrinsic excitonic transitions of semiconducting (S_{11}, S_{22}, S_{33}) and metallic (M_{11}, M_{22}) SWNTs can be clearly seen in these spectra, and their relative weighting varies as the fraction of each type of nanotube is varied. The right side of Figure 1 shows 2 × 2 μm AFM images of metal-enriched and semiconductor-enriched films. Each film comprises long, narrow bundles of tubes interwoven with a high density of junctions between bundles. The fraction of m-SWNTs

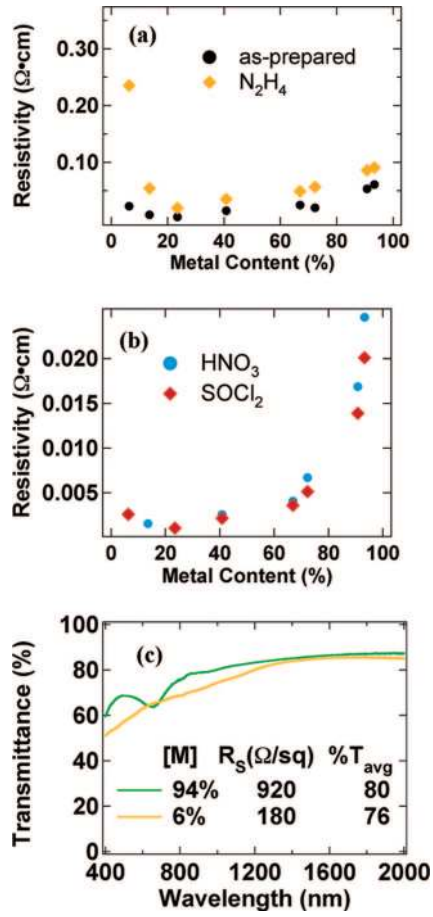

Figure 2. Dependence of film resistivity as a function of m-SWNT content for (a) as-prepared and hydrazine-treated films, and (b) HNO_3- and $SOCl_2$-doped films. Resistivity is calculated as the product of sheet resistance and film thickness. (c) Transmittance spectra for two films enriched with m-SWNTs or s-SWNTs, both of which are doped with thionyl chloride. Legend shows m-SWNT content, sheet resistance (R_S), and average percent transmittance ($\%T_{avg}$) of each film. Average transmittance is calculated over the range of 400−2000 nm.

in each film is used as a relative metric by which we may evaluate type-dependent trends. The calculation of m-SWNT content is based on the integrated areas underneath the S_{22} and M_{11} peak envelopes, as described in detail in the Supporting Information. Production of such highly tunable SWNT films has not been described previously and is critical for the analysis of the film performance dependence on SWNT electronic structure described here, as well as for intelligent device design for tailored applications.

Figure 2 shows the variation of film resistivity as a function of the m-SWNT content for as-made and chemically treated films. As-made films show a slight decrease in resistivity as the m-SWNT content is initially increased, but surprisingly, the resistivity increases again as the m-SWNT content is increased above ~30%. The same general trend in resistivity with m-SWNT content is observed for the hydrazine-treated films, but the resistivity is consistently higher for all compositions. The increase in resistivity after hydrazine treatment is much larger for the low m-SWNT content films (~10 ×) than for the high m-SWNT content films (~1.25 ×).

Redox dopants such as thionyl chloride, nitric acid, and sulfuric acid have been shown to lower the Fermi level in SWNT mats or thin films.[10,20] Consistently, soaking our films in a solution of HNO_3 or neat $SOCl_2$ dramatically decreases the resistivity for all film compositions (Figure 2b). Again, this change is substantially larger for semiconductor-enriched, low m-SWNT content films than it is for the high m-SWNT content films. For samples with very low m-SWNT content, the resistivity of the hydrazine-treated films is 100 times that of the highly conductive redox-doped films, while only a factor of 4 difference is observed for the high m-SWNT contents. Figure 2c shows that, for similar transmittance across the visible and near-IR ranges of the spectrum, a doped s-SWNT film (6% m-SWNT) has significantly lower sheet resistance than a similarly doped 94% m-SWNT film. Surprisingly, in all cases, highly metal-enriched films are out-performed by redox-doped semiconductor-enriched films. Interestingly, the shape of Figure 2b suggests that the p-doped s-SWNTs form the least resistive pathways for electronic conduction in doped SWNT networks. These trends are extremely reproducible and were seen for several different experimental conditions (see Supporting Information).

To understand the dependence of film electrical properties on the ratio of m- and s-SWNTs, we must consider the numerous factors that may impact each film's conductivity. The most obvious factor is the difference in intrinsic conductivity for s-SWNTs and m-SWNTs, based on their different electronic structures. Intrinsic, undoped s-SWNTs have essentially no carriers at the Fermi level, while m-SWNTs have appreciable carrier density at the Fermi level, owing to the nonzero density of states between the first van Hove singularities. Additionally, the carrier density injected by a redox dopant into a SWNT strongly depends on the redox potential of the dopant and the specific electronic structure of the SWNT. The junctions between nanotubes and/or nanotube bundles may also play a significant role in the transport properties of the films. The intersections of two SWNTs, regardless of type, form tunneling barriers for carriers, while junctions between m- and s-SWNTs form Schottky barriers.[9] Thus, even if significant carrier density is available for conduction at the single-tube level, the properties of tube−tube barriers influence the degree of carrier delocalization over the bulk of the film. Of course, extrinsic factors such as film morphology, non-nanotube (*e.g.*, amorphous) carbon content, and residual surfactant may also impact the optoelectronic properties of the films.

Differences in tube length, junction density, and the density of residual amorphous carbon could affect the morphology and electrical transport properties of the films. However, as shown in Figure 1, the metal- and

semienriched films appear similar by AFM. We note that we have not obtained length distributions by AFM for the s- and m-SWNTs studied in this report. However, we emphasize that comparisons such as the one shown in Figure 2 are only valid for SWNTs that have undergone the exact same sonication conditions. In fact, the separated SWNTs used to generate the films described in Figure 2 were all extracted from the same density gradient, except for the highly enriched s-SWNT film, which was extracted from a density gradient using a different surfactant ratio. Since it is unexpected for the same sonication conditions to cut s-SWNTs and m-SWNTs to dramatically different lengths, this methodology ensures a valid comparison. In some cases, when sonication times were longer, morphological differences and different magnitudes of the resistivities were observed (see Supporting Information), but the same trends shown in Figure 2 were always found. Thus, although changes in sonication can lead to differing length distributions,[21] we can conclude that variations in tube length between s- and m-SWNTs and overall film morphology are relatively insignificant to the main findings presented in this report.

Another factor that could influence film conductivity is the presence of residual surfactant, which could block transport between nanotubes at junctions. In fact, a recent report suggested that the conductivity of nitric-acid-treated SWNT thin films increased nearly 3-fold due to the removal of surfactant.[22] We also found that residual surfactant is removed by nitric acid treatment (see Supporting Information), but the doping-induced changes we observed were all completely reversible. This reversibility implies that the large conductivity enhancement induced by nitric acid soaking cannot be attributed solely to surfactant removal. We thus conclude that the main optical and electrical effects from the various chemical treatments may be best evaluated in the context of changes to the intrinsic resistance of s- and m-SWNTs, as well as the junction resistances, as described below.

To gain more insight into the origins of the electrical changes reported in Figure 2, we followed changes in the optical spectra for two highly enriched films as a function of chemical treatment, as shown in Figure 3. In the semiconductor-enriched film (Figure 3a), we observed that significant oscillator strength for the S_{11} and S_{22} transition envelopes is bleached in the as-made film but returns upon treatment with hydrazine. Concomitant with the restoration of the full oscillator strength, the sheet resistance increases 10-fold. The as-made films are likely doped p-type in laboratory air,[11] which reduces the electron density in s-SWNTs and lowers the Fermi level into the valence band. Hydrazine reverses this oxidation by the addition of electrons,[23] returning the Fermi level to the middle of the gap and restoring the semiconducting excitonic transitions.[24,25] If the hydrazine-treated films are left in air, they again

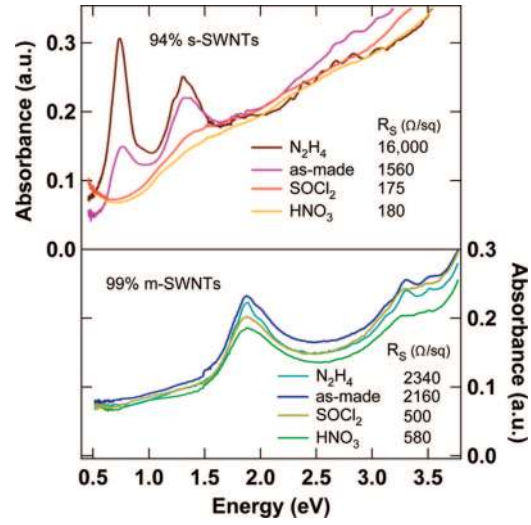

Figure 3. Absorbance spectra of s-SWNT (top) and m-SWNT (bottom) enriched films after different chemical treatments (or as-prepared).

become oxidized (showing bleached absorption peaks and increased conductivity) on a time scale of days. The effect is reversed by subsequent hydrazine treatment.

It is clear that both p-type dopants, $SOCl_2$ and HNO_3, remove essentially all oscillator strength from the S_{11} and S_{22} peak envelopes in the semiconductor-enriched films. This optical bleaching is accompanied by a dramatic decrease in the sheet resistance to ~180 Ω/sq, a change of nearly 2 orders of magnitude compared to the hydrazine-treated film. At the low energy side of the spectrum, the tail of a new doping-induced absorbance feature can be seen rising into the infrared. Similar to the oxygen doping effect, these optical and electrical changes are all completely reversible upon cycling hydrazine and p-type dopant treatments. These changes are explained by redox-mediated charge trans-

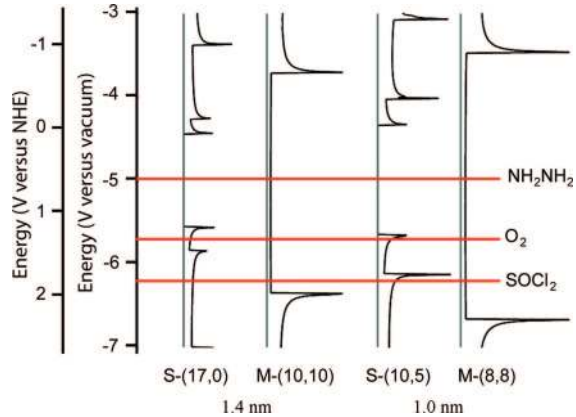

Figure 4. Calculated density of states for (17,0) and (10,5) s-SWNTs and (10,10) and (8,8) m-SWNTs, representative of the 1−1.4 nm diameter distribution produced by laser vaporization, plotted on an absolute energy scale, *versus* the normal hydrogen electrode (NHE) and *versus* vacuum. Red lines show the approximate Fermi level following intentional (hydrazine and thionyl chloride) chemical treatments and unintentional oxygen adsorption. The Fermi level positions are estimated based on chemically induced optical and electrical changes, as discussed in the text.

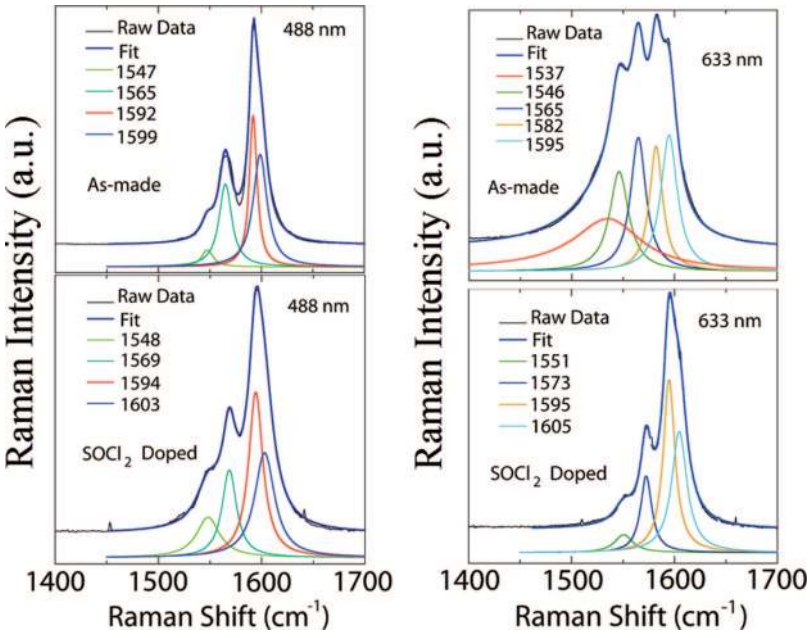

Figure 5. Raman spectra of as-prepared (top panels) and $SOCl_2$-doped (bottom panels) SWNT films in the tangential (G-band) region. Left panels show s-SWNT film (6% m-SWNTs). The excitation wavelength was 488 nm, and the excitation power was 3 mW. Right panel shows a m-SWNT film (97% m-SWNTs). The excitation wavelength was 633 nm, and the excitation power was 6 mW. Individual peaks from multi-Lorentzian fits are offset below the raw data and fits for clarity, and Raman shifts of individual peaks are shown in the legend. The broad peak at 1537 cm^{-1} for the as-prepared m-SWNT film excited at 633 nm was fit with a BWF line shape.

fer from semiconducting SWNTs to the p-type dopants, which lowers the Fermi level near or below the second van Hove singularity in the valence band.[10] The SWNT free carrier plasma frequency, ω_p, is related to the carrier concentration *via* $\omega_p^2 = 4\pi pe^2/m*$, where p is the hole concentration, and $m*$ is the effective mass. Consistently, the plasma edge appears in the near-IR.[10]

The optical and electrical changes observed for the metal-enriched films are much less pronounced. Treatment with hydrazine does not add appreciable oscillator strength to the M_{11} or M_{22} transitions and only slightly increases the sheet resistance by ~8% relative to the as-made film, suggesting that ambient oxidation of m-SWNTs does not remove electron density directly from metallic van Hove singularities. Upon doping with $SOCl_2$ or HNO_3, the M_{11} and M_{22} peak envelopes are broadened and lose some of the fine structure arising from individual m-SWNT transitions but do not suffer a significant loss (<5%) of integrated optical density, indicating that the redox potentials of the dopant molecules are not positive of the M_{11} hole level. The adsorbed dopants do, however, lead to a significant broadening of the M_{11} and M_{22} peak envelopes, which can be explained by a Stark-induced broadening and shifting of the individual transitions that comprise these envelopes.[26] Similar to the semiconductor-enriched films, all of the optical and electrical changes are completely reversible.

These changes in the optical spectra allow us to approximate the Fermi level position for each of the treatments studied here, as shown in the calculated density of states in Figure 4. The Fermi level for the hydrazine-treated SWNTs is in the middle of the gap, such that the s-SWNTs and m-SWNTs within any particular film may be considered intrinsic. "Unintentional" doping by ambient oxidation moves the Fermi level near or slightly below the S_{11} hole level, while the Fermi level of the intentionally doped SWNT films lies below the S_{22} level and above the M_{11} hole level.

The dopant hole density, n_D, imparted by redox doping can be estimated by

$$n_D = \int_{E_1}^{E_2} \mathrm{DOS}(E)\mathrm{d}E \qquad (1)$$

where E_1 is taken to be the intrinsic Fermi energy and E_2 is the new Fermi level induced by the redox dopants. For the DOS shown in Figure 4, we find that $SOCl_2$ doping introduces 0.016−0.018 delocalized holes per carbon atom for s-SWNTs, while for the m-SWNTs, the range is 0.011−0.013. Thus, the hole density imparted by redox doping into individual SWNTs is ~42% higher for s-SWNTs than for m-SWNTs.

We note here that Raman spectroscopy is often used to estimate the free carrier density injected by redox dopants[15] but point out that the charge transfer density estimated from such analyses may vary widely depending on the reference value used and, possibly, even the Raman laser's resonance conditions. For example, Sumanasekera *et al.* studied H_2SO_4-doped SWNTs and found a reproducible blue shift, $d\omega/df$, of ~320 cm^{-1} per hole per carbon atom for the G band of the redox-doped SWNTs.[27] In contrast, the work of Eklund *et al.* on H_2SO_4-treated graphite found a stronger E_{2g} dependence of ~1050 cm^{-1} per hole per carbon atom.[28] Figure 5 shows Raman spectra before and after doping with $SOCl_2$ for semiconductor-enriched and metal-enriched films. The blue shifts we observe in the Raman G-band peaks for thionyl-chloride-doped films range from 1 to 13 cm^{-1}. Using the two references from above, we would calculate an injected hole density anywhere from 0.001 to 0.04 holes per carbon atom, a wide range that does not allow for an unambiguous assessment. Interestingly, for the small shifts (1−4 cm^{-1}) observed for 488 nm excitation, which is predominantly resonant with s-SWNTs, our calculations correlate best with Sumaneseskera's SWNT study at a similar excitation wavelength (514.5 nm).[27] In contrast, the large shifts (5−13 cm^{-1}) observed for 633 nm excitation, which is predominantly resonant with m-SWNTs,

correlate better with Eklund's study on stage 2 intercalated graphite.[28]

While our calculation provides a reliable estimation of the density of holes induced by the redox reaction with the individual tubes, all of these carriers may not contribute to the DC conductivity of the film. In fact, two pieces of evidence strongly suggest that all carriers at the single-tube level do not contribute to long-range transport: (1) the DC conductivity of the m-SWNT film is several orders of magnitude lower than expected by considering the total carrier density within the conduction band of individual m-SWNTs (approximately 1 electron per carbon atom) and (2) upon redox doping the m-SWNT film, the carrier density increases by only 1% at the single-tube level, but the resistivity decreases more dramatically, by a factor of 4. These observations are not consistent with a film dominated by delocalized metallic conduction. We suggest that interactions associated with tube−tube junctions primarily control the resistivity in these films. The FET mobility in single SWNTs (intrinsic m-SWNTs or s-SWNTs in the "on" state) is extremely high, on the order of 1000−10 000 $cm^2/V \cdot s$, resulting in mean free path lengths of the order of 0.5 to several microns (assuming a effective mass of 1 and Fermi velocity of 8×10^5 m/s). Since this distance is much longer than the typical distance between tube−tube junctions, it is reasonable to conclude that the unexpectedly high resistance of the SWNT films is due to the large density of tube−tube junctions. Each junction creates a tunnel barrier through which electrons must propagate with some finite transmission probability. Therefore, carriers localized on one SWNT may either tunnel into an adjacent SWNT with some probability that depends upon tube−tube barriers or remain localized upon the SWNT. Those carriers that remain localized do not contribute to DC transport, while the delocalized carriers do.

With this model in mind, we performed temperature-dependent transport measurements, shown in Figure 6. For both the s-SWNT and m-SWNT films, as the temperature is raised from 100 K to room temperature, the sheet resistance decreases with an exponential dependence. The temperature-dependent resistance data strongly support the hypothesis that intertube junctions limit the conductivity of these transparent SWNT films. Figure 6b demonstrates a progressive decrease in resistance with increasing temperature for the m-SWNT film, an effect seen in conducting polymers and bulk SWNT films, but not expected for a film with purely metallic conduction. The temperature dependence of transport in SWNT networks is typically described by considering metallic regions of conductivity separated by thin tunneling barriers.[14,29] This behavior is often modeled by a generalized equation similar to eq 2:

$$R_S = \alpha T + \beta \exp\left|\frac{T_b}{T_s + T}\right| \quad (2)$$

In eq 2, the linear term represents metal-like conductivity and the second term represents the tunneling contribution. The tunneling term in eq 2 was used to fit the temperature-dependent data shown in Figure 6, and the fits are shown as solid lines.

A complete analysis of temperature-dependent resistivity is forthcoming (Barnes *et al.*), but the fits shown for these two films provide critical metrics with which to analyze the effect of SWNT electronic structure and redox doping on the tube−tube barriers. Specifically, the T_b parameter is a function of the tunnel barrier height and shape as affected by the image force and local field.[30] Upon p-type doping, T_b is significantly lowered for both semiconductor- and metal-enriched films. If barrier energies are lowered *via* chemical modification, conductance through the barriers increases and the exponential temperature dependence becomes more shallow.[10] Thus, we conclude that $SOCl_2$, HNO_3, or O_2 molecules adsorbed at or near tube−tube junctions create local electric fields that lower the tunnel barriers, increasing the conductance through junctions and increasing the degree of carrier delocalization. Figure 6 demonstrates that T_b is reduced for the semiconductor-enriched films to a greater degree than for the metal-enriched films, which suggests that the p-type dopants increase conductance through tunnel junctions between s-SWNTs more effectively than junctions between m-SWNTs.

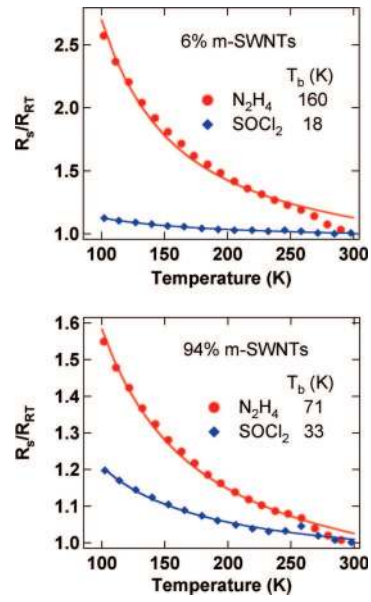

Figure 6. Temperature dependence of the sheet resistance for s-SWNT (top) and m-SWNT (bottom) enriched films as a function of chemical treatment. The sheet resistance is normalized to the sheet resistance at 300 K for comparative purposes. Points are experimental data, and solid lines are fits to eq 2. The legend in each panel displays the T_b constant obtained for the fit to each data set.

The data shown here allow for a consistent description of the tunable transparent conductive SWNT films. The films are best described as three-dimensional networks of highly conductive (at the single-tube level) quantum wires with tunnel barriers between individual wires. As such, the critical factors for determining film conductivity are (1) the density of carriers available for conduction, (2) the degree of carrier delocalization as affected by tube−tube barriers, and (3) the effect that redox doping has on each of these parameters. For hydrazine-treated s-SWNTs, the Fermi level is in the middle of the gap, meaning virtually no carriers are available for conduction. As a result, percolation pathways are formed by m-SWNTs in intrinsic, undoped, mixed films containing both s- and m-SWNTs. The small conductivity that is measured for the intrinsic s-SWNT film may arise from the small amount of m-SWNTs that form a percolation path, oxygen doping resulting from the short ambient exposure after hydrazine treatment, or a small amount of delocalized carriers created by SWNT defects.

Intrinsic m-SWNT films have significant free carrier density at the single-tube level, but, in a three-dimensional network, highly reflective intertube barriers cause the majority of these carriers to remain localized to individual SWNTs. The low density of delocalized carriers that may propogate within the entire m-SWNT film prevents the realization of the enhanced conductivities one might expect in going from bulk SWNT films (1/3 m-SWNTs) to films made of nearly 100% m-SWNTs.

From the shape of Figure 2b, it is evident that p-doped s-SWNTs form the least resistive conductive pathways for intentionally redox-doped films. $SOCl_2$ and HNO_3 redox dopants inject large hole densities into individual s- and m-SWNTs, as shown in Figure 4. However, the propensity for this large carrier density to contribute to the film conductivity critically depends on the transmission probability through intertube barriers. As shown here, the p-type redox dopants inject a larger hole density into individual s-SWNTs relative to m-SWNTs and modify intertube barriers such that more of these injected carriers are delocalized over the bulk of the film. For these reasons, the doped s-SWNT films are consistently more conductive than intrinsic or doped m-SWNT films.

Since the conditions of this study closely mimic the conditions utilized for producing conductive bulk SWNT transparent electrodes (Supporting Information), we conclude that conventionally produced, doped SWNT transparent electrodes[18,31] are dominated by the percolation of doped s-SWNTs, in contrast to the conventional wisdom that percolation pathways are formed by m-SWNTs. Note that our conclusions are in agreement with FET studies that have shown that s-SWNTs have very high mobilities, of the same magnitude of m-SWNTs, in their "on state" in which holes are localized in the s-SWNT valence band by a strong applied field.[4,5,32] Also, it has been found that junctions between s-SWNTs have comparable transmission probabilities to junctions formed between m-SWNTs.[9] These observations suggest that degenerately doped s-SWNTs have similar transport parameters to intrinsic m-SWNTs and should likewise form conductive percolation pathways in thin SWNT films. Essentially, the two should be interchangeable in models where metallic conduction is assumed to dominate the transport behavior in three-dimensional SWNT networks.

Finally, our results do not imply that highly conductive m-SWNT films cannot be realized. Our data suggest that the primary factor reducing the conductivity for m-SWNT networks is the junction resistance and/or tube−tube electronic coupling, implying that intelligent control of junction density (as low as possible) and energy profile (possibly minimized by nonvolatile chemical cross-linking) may be fruitful avenues for increasing conductivity in these films. Ultimately, highly conductive m-SWNT transparent films may be preferable to s-SWNT films because the conductivity should not be controlled by volatile chemicals, a drawback for doped s-SWNT films in any devices requiring high temperature fabrication.

METHODS

Synthesis and Density Gradient Separation of SWNTs. Single-walled carbon nanotubes (SWNTs) were produced by laser vaporization using nitrogen as the carrier gas. Separation of metallic and semiconducting SWNTs (m-SWNTs and s-SWNTs, respectively) was achieved by density gradient centrifugation in a cosurfactant mixture, following a recently published procedure.[16] The two surfactants used were sodium cholate (SC) and sodium dodecyl sulfate (SDS). For the films discussed in this paper, we sonicated ~20 mg of raw laser soot in 20 mL of an aqueous cosurfactant solution of 3:2 SDS:SC or 4:1 SC:SDS. As discussed in the Supporting Information (Figures S2a−c), we also performed experiments where we first sonicated in only one surfactant, SC, and then adjusted to 3:2 SDS:SC or 4:1 SC:SDS afterward. As shown in the Supporting Information, sonication in a single surfactant (SC), followed by addition of the co-surfactant (SDS), produced results similar to those of sonication in the cosurfactant mixture. As described previously,[16] the total surfactant concentration was 2% (w/v), while the ratio of surfactants determined the specific density profile of metallic and semiconducting species. A Cole Palmer 750 W sonication was used, with a 1/4 in. ultrasonic tip. The dispersions discussed in the text were sonicated for 10 min at 30% power while the sample was cooled by 20 °C water flowing in an external jacket. As discussed in the Supporting Information, other sonication powers and durations were tested for their effects on resistivity and transparency trends. As mentioned in the text and shown by Figures S2a−c and S3 in the Supporting Information, the trends, as a function of m-SWNT, were the same regardless of the sonication conditions.

Prior to density gradient centrifugation, an appropriate amount of iodixanol was added to the solution, and this bulk solution was then injected ~5/6 of the way down a linear 10 mL density gradient. The bottom ~3 mL of the centrifuge tube is 52% iodixanol, while the top ~10 mL contains no iodixanol. For m-SWNT separations, a 3:2 (SDS:SC) surfactant ratio was used, and centrifugation was done at 47 000 rpm in a Ti70 rotor for 13 h; for s-SWNT separations, a 4:1 (SC:SDS) ratio was used, and centrifugation was done at 41 000 rpm in the same rotor for 15 h.

Estimation of m-SWNT Content and Formation of Films with Precisely Tunable m-SWNT Content. Following centrifugation of a "m-SWNT separation", a ~2 mm blue band, corresponding to m-SWNTs, lies well-separated above darker brown bands corresponding to s-SWNTs. Alternatively, for "s-SWNT separations", the top band was yellow-brown and enriched with s-SWNTs. Successive aliquots of ~300−500 μL are removed from the top down with a syringe topped with a flat-tipped needle. These aliquots contain a varied proportion of m- and s-SWNTs, according to their position in the density gradient and the amount of unintentional mixing. We estimate the relative proportions of m- and s-SWNTs by comparing M_{11} and S_{22} peak intensities in the visible absorbance spectrum, as discussed in detail in the Supporting Information. We then combine the appropriate volumes of specifically chosen fractions to span a wide range of metal/semiconductor ratios. The films created from these solutions are found to have m-SWNT contents ranging from ~3 to ~99%, as determined by integration of the M_{11} and S_{22} areas (Figure S4).

Transparent conductive films are formed by the method described by Wu *et al.*[18] Solutions are diluted to ~20 mL with water and sonicated briefly (10 min) with a cup-horn sonicator before filtering through a mixed cellulose ester (MCE) filter. The MCE cross section exposed to the filtrate consists of a circle with ~1 cm diameter. In general, the conditions are selected so that we achieve an optical density of ~0.2 (~63% T) at the peak of the M_{11} or S_{22} transition (without background subtraction, see Supporting Information and Figure S5). We estimate the mass of SWNTs necessary to form such a film is ~5−10 μg. After formation of the film on the MCE membrane, the SWNT film is transferred to a glass or quartz substrate by first wetting the membrane with water and applying it to the substrate, SWNT film side on the substrate. The substrate is then heated in an acetone vapor bath for ~10 min to liquefy the MCE membrane and achieve full adhesion of the SWNT film to the substrate. Residual MCE is washed away by soaking the film/substrate in acetone overnight.

As a point of reference to other reports, a purified, nitric acid doped bulk film (1/3 m-SWNTs, 2/3 s-SWNTs) prepared in such a manner at our laboratory has a sheet resistance of ~100−250 Ω/sq with average transmittance (400−1000 nm) of ~80−85% (Figure S6 in Supporting Information). These metrics are on par with the best SWNT conductive films from the literature.

Atomic Force Microscopy Measurement of Film Thickness. Film thicknesses were measured for several films using AFM. The AFM tip was rastered over a 10 × 10 μm area, half of which was covered by the thin SWNT film, while the other half was bare quartz. From these thicknesses, and the m- and s-SWNT percentages determined for these films, as discussed above, integrated extinction coefficients (per unit thickness) were calculated for the M_{11} and S_{22} bands. We then were able to estimate the thicknesses of all other films optically, using the integrated extinction coefficients determined above. Thickness values for films in this study ranged from 50 to 100 nm. The films in the main text have an average thickness of 42 ± 10 nm.

Chemical Film Treatments. For redox doping, films were immersed in either a 4 M solution of nitric acid or neat thionyl chloride for anywhere from 4 to 24 h. Beyond ~4 h, the exact duration of soaking was found to be unimportant. To "de-dope" films, the as-prepared or redox-doped films were soaked in a 1 M solution of hydrazine in ethanol. Approximately 4 h was also found to be sufficient for the hydrazine chemical treatment. The films discussed in the paper were treated in the following order: (1)filtration and transfer to glass → as-prepared film; (2) overnight soak in 4 M HNO_3 → nitric-doped film; (3) overnight soak in N_2H_4 → intrinsic film; (4) overnight soak in $SOCl_2$ → thionyl chloride doped film; (5) iterations of N_2H_4 and redox dopants for reversibility studies. This order is critical to achieving efficient doping by $SOCl_2$, as shown in Figure S7. If excess surfactant is not washed away by the HNO_3 treatment, insufficient intercalation of $SOCl_2$ molecules can be a problem.

Computation Methods. We used VASP[33] and SIESTA[34] to study electronic structures of various single-wall carbon nanotubes within the local density approximation (LDA).[35] For plane-wave VASP calculations, we used the kinetic energy cutoff of 400 eV. LDA and experimental energy gaps of seven semiconducting chiral nanotubes were compared as shown in Figure S1 with diameters ranging from 7.6 to 10.5 Å.[36] LDA underestimates the real electronic gaps by about 57.4% on average. For electronic density of states (DOS) of individual single-wall nanotubes, we used SIESTA to get one-dimensional band structures with double ζ-polarization (DZP) basis sets and take $DOS^{LDA}(E) = 2\sum dk/dE$, where the factor of 2 is for spin degeneracy and the summation runs over all bands. The $DOS^{LDA}(E)$ was scaled down by multiplying 0.574 as the LDA energy is smaller by 1.74 times than experiment. Figure 4 shows the corrected DOS of (10,10), (17,0), (8,8), and (10,5) nanotubes. The former two have diameters of 1.4 nm, and the latter two have diameters of 1 nm, corresponding to two extremes of laser tubes. Oxidation states have been calculated by integrating the DOS from −6.5 to −5 eV, and the redox-injected hole density is calculated by normalizing the charge density removed by the dopants to a per-carbon-atom basis.

Acknowledgment. This work was funded by the U.S. Department of Energy's Solar Photochemistry Program within the Office of Science, Office of Basic Energy Sciences, Division of Chemical Sciences, Geosciences, and Biosciences, under contract number DE-AC36-99GO10337 to NREL, as well as the Department of Energy's Laboratory Directed Research and Development fund. We would also like to thank Martha Symko-Davies and the High Efficiency Concepts Program for Funding.

Supporting Information Available: Additional experimental details. This material is available free of charge *via* the Internet at http://pubs.acs.org.

REFERENCES AND NOTES

1. Du Pasquier, A.; Unalan, H. E.; Kanwal, A.; Miller, S.; Chhowalla, M. Conducting and Transparent Single-Wall Carbon Nanotube Electrodes for Polymer-Fullerene Solar Cells. *Appl. Phys. Lett.* **2005**, *87*, 203511/1–203511/3.
2. van de Lagemaat, J.; Barnes, T. M.; Rumbles, G.; Shaheen, S. E.; Coutts, T. J. Organic Solar Cells with Carbon Nanotubes Replacing ITO as the Transparent Electrode. *Appl. Phys. Lett.* **2006**, *88*, 233503/1–233503/3.
3. Contreras, M. A.; Barnes, T.; van de Lagemaat, J.; Rumbles, G.; Coutts, T. J.; Weeks, C.; Glatkowski, P.; Levitsky, I.; Peltola, J.; Britz, D. A. Replacement of Transparent Conductive Oxides by Single-Wall Carbon Nanotubes in $Cu(In,Ga)Se_2$-Based Solar Cells. *J. Phys. Chem. C* **2007**, *111*, 14045–14048.
4. Javey, A.; Guo, J.; Wang, Q.; Lundstrom, M.; Dai, H. Ballistic Carbon Nanotube Field-Effect Transistors. *Nature* **2003**, *424*, 654–657.
5. Kong, J.; Yenilmez, E.; Tombler, T. W.; Kim, W.; Dai, H.; Laughlin, R. B.; Liu, L.; Jayanthi, C. S.; Wu, S. Y. Quantum Interference and Ballistic Transmission in Nanotube Electron Waveguides. *Phys. Rev. Lett.* **2001**, *87*, 106801/1–106801/4.
6. Cao, Q.; Hur, S.-H.; Zhu, Z.-T.; Sun, C.-J.; Wang, C.-J.; Meitl, M. A.; Shim, M.; Rogers, J. A. Highly Bendable, Transparent Thin-Film Transistors That Use Carbon-Nanotube-Based Conductors and Semiconductors with Elastomeric Dielectrics. *Adv. Mater.* **2006**, *18*, 304–309.
7. Xu, H.; Anlage, S. M. Microwave Shielding of Transparent and Conducting Single-Walled Carbon Nanotube Films. *Appl. Phys. Lett.* **2007**, *90*, 183119/1–183119/3.
8. Kaiser, A. B.; Dusberg, G.; Roth, S. Heterogeneous Model for Conduction in Carbon Nanotubes. *Phys. Rev. B* **1998**, *57*, 1418–1421.

9. Fuhrer, M. S.; Nygard, J.; Shih, L.; Forero, M.; Yoon, Y.-G.; Mazzoni, M. S. C.; Choi, H. J.; Ihm, J.; Louie, S. G.; Zettl, A.; McEuen, P. L. Crossed Nanotube Junctions. *Science* **2000**, *288*, 494–497.
10. Zhou, W.; Vavro, J.; Nemes, N. M.; Fischer, J. E.; Borondics, F.; Kamaras, K.; Tanner, D. B. Charge Transfer and Fermi Level Shift in p-doped Single-Walled Carbon Nanotubes. *Phys. Rev. B* **2005**, *71*, 205423/1–205423/7.
11. Collins, P. G.; Bradley, K.; Ishigami, M.; Zettl, A. Extreme Oxygen Sensitivity of Electrical Properties of Single-Wall Carbon Nanotubes. *Science* **2001**, *287*, 1801–1804.
12. Skakalova, V.; Kaiser, A. B.; Dettlaff-Weglikowska, U.; Hrncarikova, K.; Roth, S. Effect of Chemical Treatment on Electrical Conductivity, Infrared Absorption, and Raman Spectra of SWCNT. *J. Phys. Chem. B* **2005**, *109*, 7174–7181.
13. Kocabas, C.; Pimparkar, N.; Yesilyurt, O.; Kang, S. J.; Alam, M. A.; Rogers, J. A. Experimental and Theoretical Studies of Transport through Large Scale, Partially Aligned Arrays of Single-Walled Carbon Nanotubes in Thin Film Type Transistors. *Nano Lett.* **2007**, *7*, 1195–1202.
14. Skakalova, V.; Kaiser, A. B.; Woo, Y. S.; Roth, S. Electronic Transport in Carbon Nanotubes: From Individual Nanotubes to Thin and Thick Networks. *Phys. Rev. B* **2006**, *74*, 085403/1–085403/10.
15. Miyata, Y.; Yanagi, K.; Maniwa, Y.; Kataura, H. Highly Stabilized Conductivity of Metallic Single Wall Carbon Nanotube Thin Films. *J. Phys. Chem. C* **2008**, *112*, 3591–3596.
16. Arnold, M. S.; Green, A. A.; Hulvat, J. F.; Stupp, S. I.; Hersam, M. C. Sorting Carbon Nanotubes by Electronic Structure Using Density Differentiation. *Nat. Nanotechnol.* **2006**, *1*, 60–65.
17. Itkis, M. E.; Perea, D. E.; Niyogi, S.; Rickard, S. M.; Hamon, M. A.; Hu, H.; Zhao, B.; Haddon, R. C. Purity Evaluation of As-Prepared Single-Walled Carbon Nanotube Soot by Use of Solution-Phase Near-IR Spectroscopy. *Nano Lett.* **2003**, *3*, 309–314.
18. Wu, Z.; Chen, Z.; Du, X.; Logan, J. M.; Sippel, J.; Nikolou, M.; Kamaras, K.; Reynolds, J. R.; Tanner, D. B.; Hebard, A. F.; Rinzler, A. G. Transparent, Conductive Carbon Nanotube Films. *Science* **2004**, *305*, 1273–1276.
19. Nair, N.; Usrey, M. L.; Kim, W.-J.; Braatz, R. D.; Strano, M. S. Estimation of the (n,m) Concentration Distribution of Single-Walled Carbon Nanotubes from Photoabsorption Spectra. *Anal. Chem.* **2006**, *78*, 7689–7696.
20. Dettlaff-Weglikowska, U.; Skakalova, V.; Graupner, R.; Jhang, S. H.; Kim, B. H.; Lee, H. J.; Ley, L.; Park, Y. W.; Berber, S.; Tomanek, D.; Roth, S. Effect of $SOCl_2$ Treatment on Electrical and Mechanical Properties of Single-Wall Carbon Nanotube Networks. *J. Am. Chem. Soc.* **2005**, *127*, 5125–5131.
21. Islam, M. F.; Rojas, E.; Bergey, D. M.; Johnson, A. T.; Yodh, A. G. High Weight Fraction Surfactant Solubilization of Single-Wall Carbon Nanotubes in Water. *Nano Lett.* **2003**, *3*, 269–273.
22. Geng, H.-Z.; Kim, K. K.; So, K. P.; Lee, Y. S.; Chang, Y.; Lee, Y. H. Effect of Acid Treatment on Carbon Nanotube-Based Flexible Transparent Conducting Films. *J. Am. Chem. Soc.* **2007**, *129*, 7758–7759.
23. Klinke, C.; Chen, J.; Afzali, A.; Avouris, P. Charge Transfer Induced Polarity Switching in Carbon Nanotube Transistors. *Nano Lett.* **2005**, *5*, 555–558.
24. Blackburn, J. L.; McDonald, T. J.; Metzger, W. K.; Engtrakul, C.; Rumbles, G.; Heben, M. J. Protonation Effects on the Photoluminescence Quantum Yield and the Branching Ratio in Photoexcited SWNT Dispersions. *Nano Lett.* **2008**, *8*, 1047–1054.
25. We note that reference 23 (Klinke) demonstrated that hydrazine can inject electrons into the s-SWNT LUMO, producing n-type FETs when measured in an inert atmosphere. In our experiments, the hydrazine-treated films are exposed to air before characterization. Under these conditions, any electrons injected into the s-SWNT LUMO would be rapidly quenched by oxygen, and we may consider the Fermi level to be approximately mid-gap.
26. Each site at which a redox molecule is adsorbed to the SWNT surface constitutes a discrete ion pair with an associated dipole. Each dipole creates an electric field, which alters the SWNT electronic structure, affecting the peak width and energy of interband transitions. This stark effect would serve to broaden and smear out the M_{11} and M_{22} peak envelopes even if electrons were not directly transferred from these levels to the p-type dopants.
27. Sumanasekera, G. U.; Allen, J. L.; Fang, S. L.; Loper, A. L.; Rao, A. M.; Eklund, P. C. Electrochemical Oxidation of Single Wall Carbon Nanotube Bundles in Sulfuric Acid. *J. Phys. Chem. B* **1999**, *103*, 4292–4297.
28. Eklund, P. C.; Arakawa, E. T.; Zarestky, J. L.; Kamitakahara, W. A.; Mahan, G. D. Charge-Transfer-Induced Changes in the Electronic and Lattice Vibrational Properties of Acceptor-type GICs. *Synth. Met.* **1985**, *12*, 97–102.
29. Fischer, J. E.; Dai, H.; Thess, A.; Lee, R.; Hanjani, N. M.; Dehaas, D. L.; Smalley, R. E. Metallic Resistivity in Crystalline Ropes of Single-Wall Carbon Nanotubes. *Phys. Rev. B* **1997**, *55*, R4921−R4924.
30. Sheng, P. Fluctuation-Induced Tunneling Conduction in Disordered Materials. *Phys. Rev. B* **1980**, *21*, 2180–2195.
31. Zhang, D.; Ryu, K.; Liu, X.; Polikarpov, E.; Ly, J.; Tompson, M. E.; Zhou, C. Transparent, Conductive, and Flexible Carbon Nanotube Films and Their Application in Organic Light-Emitting Diodes. *Nano Lett.* **2006**, *6*, 1880–1886.
32. Durkop, T.; Kim, B. M.; Fuhrer, M. S. Properties and Applications of High-Mobility Semiconducting Nanotubes. *J. Phys.: Condens. Matter* **2004**, *16*, R553−R580.
33. Kresse, G.; Joubert, J. From Ultrasoft Pseudopotentials to the Projector Augmented-Wave Method. *Phys. Rev. B* **1999**, *59*, 1758–1775.
34. Soler, J. M.; Artacho, E.; Gale, J. D.; Garcia, A.; Junquera, J.; Ordejon, P.; Sanchez-Portal, D. The SIESTA Method for *ab initio* Order-N Materials Simulation. *J. Phys.: Condens. Matter* **2002**, *14*, 2745–2779.
35. Ceperly, D. M.; Alder, B. I. Ground State of the Electron Gas by a Stochastic Method. *Phys. Rev. Lett.* **1980**, *45*, 566–569.
36. McDonald, T. J.; Svedruzic, D.; Kim, Y.-H.; Blackburn, J. L.; Zhang, S. B.; King, P.; Heben, M. J. Wiring Up Hydrogenase with Single-Walled Carbon Nanotubes. *Nano Lett.* **2007**, *7*, 3528–3534.